Author(s): Ganchenkova, M. G. & Borodin, V. A. & Laaksonen, K. & Nieminen, Risto M.

Title: Modeling the compositional instability in wurtzite Ga1-x InxN

Year: 2008

Version: Final published version

Please cite the original version:

Ganchenkova, M. G. & Borodin, V. A. & Laaksonen, K. & Nieminen, Risto M. 2008. Modeling the compositional instability in wurtzite Ga1-x InxN. Physical Review B. Volume 77, Issue 7. 075207/1-13. ISSN 1550-235X (electronic). DOI: 10.1103/physrevb.77.075207.

Modeling the compositional instability in wurtzite $Ga_{1-x}In_xN$

M. G. Ganchenkova,[1] V. A. Borodin,[2] K. Laaksonen,[1] and R. M. Nieminen[1]
[1]*COMP/Laboratory of Physics, Helsinki University of Technology, P.O. Box 1100, 02015 Espoo, Finland*
[2]*RRC Kurchatov Institute, Kurchatov Square 1, 123182 Moscow, Russia*
(Received 4 November 2007; published 26 February 2008)

The paper deals with multiscale modeling of the minor component ordering in wurtzite $Ga_{1-x}In_xN$ ($x<0.5$) alloys. The treatment combines the total-energy density-functional calculations of the metal atom interaction parameters and the atomistic description of the alloy decomposition using lattice kinetic Monte Carlo. It is demonstrated that the phase decomposition patterns in wurtzite GaInN are very sensitive to the interplay of metal atom interactions at several interatomic distances (at least to the fourth nearest neighbors) on the cation sublattice. Variation of the metal interaction energies within reasonable limits resulted in pronouncedly different relaxation patterns (linear or wall ordering of In and Ga atoms along *c*-axis, planar ordering parallel to basal plane, spinodal decomposition). The high sensitivity of the GaInN decomposition to relatively small variations of the metal interaction energies could be the main reason for the experimentally observed versatility of the alloy decomposition patterns and their sensitivity to the particular experimental conditions.

DOI: 10.1103/PhysRevB.77.075207 PACS number(s): 64.75.−g, 61.82.Fk, 64.60.Cn

I. INTRODUCTION

The unique properties of gallium nitride based semiconductors make them very attractive for short-wavelength light emitters and high-power and/or high-temperature electronics applications.[1] In particular, $Ga_{1-x}In_xN$ alloys are very promising because of their ability to emit light in the wavelength range from ultraviolet (GaN) to red (InN). However, a serious problem for the application of these alloys in electronic devices is their pronounced trend toward phase decomposition.[2–12] The resulting nonuniformity of the alloy chemical composition can unfavorably affect the alloy electronic properties.[13]

Phase decomposition is observed already in as-grown GaInN layers and, currently, it is a common trend to associate the observed phase decomposition with the mechanisms specific for the growth conditions.[14,15] However, thermodynamic instability seems to be the inherent property of the wurtzite modification of GaInN, because InN precipitation was observed in GaInN during high-temperature annealing as well.[7] Also, the phase separation in InGaN film, which had started at the film growth stage, was further promoted by the high-temperature postgrowth annealing,[9] which would not be the case if the decomposition was entirely a growth artifact.

Though phase decomposition of alloys is generally a well-known phenomenon, the microstructure evolution laws in GaInN alloys are not yet fully understood. GaInN demonstrates multiple, sometimes seemingly mutually contradictory, decomposition modes, including alloy ordering[8,9] and phase separation: either precipitation,[5–7] or compositional modulations.[12,16] Moreover, in some experiments, the different decomposition modes are observed simultaneously in the same alloy samples.[11]

The thermal stability of GaInN (more precisely, of its zinc-blende modification) was addressed in a number of theoretical studies, dealing with the calculation of GaInN phase diagram.[17–22] In spite of quite different expressions used for calculations of the alloy mixing energy (from the simple parabolic law of regular solution theory[17] to sophisticated cluster expansion[22]) and the ways of estimating relevant input parameters for them (from semiempirical valence-force-field approximation[17,19] to detailed first-principles calculations[22,23]), these treatments consistently predict the miscibility gap for GaInN in a broad temperature range and, thus, explain at least some trends of microstructural evolution in GaInN (precipitation and spinodal decomposition). However, these results are insufficient to explain, for instance, why phase precipitation coexists in GaInN with pronounced ordering. In fact, in terms of regular solution theory, phase decomposition and ordering are mutually exclusive in binary alloys and all thermodynamic theories treat GaInN as a quasibinary alloy, neglecting the nitrogen sublattice. Neither is it clear how to explain the appearance of ordered compositional modulations during spinodal decomposition. Hence, more sophisticated models need to be considered to explain the whole body of experimental observations.

In particular, the coexistence of phase separation and ordering can be explained, provided the mixing enthalpy includes several parabolic terms from, say, metallic atom interactions at different interatomic separations.[24,25] In this sense, the difference between zinc-blende GaInN, typically considered in phase diagram calculations, and its wurzite modification, can be important. In zinc-blende modification, the simplest approximation for the mixing enthalpy, where only metal atom interactions at the first nearest neighbor separation are taken into account, involves the sole free parameter, namely, the first-neighbor pairwise interchange energy,[26]

$$W = 2E_{\text{Ga-In}} - E_{\text{Ga-Ga}} - E_{\text{In-In}},$$

where $E_{\text{Ga-Ga}}$, $E_{\text{Ga-In}}$, and $E_{\text{In-In}}$ are the energies of pairwise interactions between nearest-neighbor atoms of corresponding types. In contrast, the metal sublattice in wurtzite GaInN is hcp with nonideal c/a ratio (from 1.626 in pure GaN to 1.612 in pure InN,[27] cf. the ideal value of 1.633). Correspondingly, a metal atom is surrounded by nearest-neighbor cation sites of two nonequivalent types—in the own basal

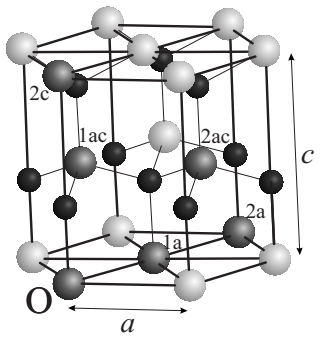

FIG. 1. The wurtzite structure of $Ga_{1-x}In_xN$ alloy. Black spheres represent nitrogen atoms, while white and shaded spheres represent metal atoms. The shading is used to mark the special dispositions of atoms considered in the paper. *a* and *c* are the basal and prismatic lattice parameters, respectively.

plane (configuration O-1a in Fig. 1) and in the neighboring basal planes (configuration O-1ac). Hence, at least two, generally different, pairwise interchange energies, W^{aa} and W^{ac}, corresponding to these configurations contribute to the free energy of the system. Moreover, in addition to the nearest neighbors, contributions from more separated metal atoms (e.g., configurations O-2ac and O-2c in Fig. 1) might give non-negligible contribution to the crystal free energy, which will additionally increase the difference between zinc-blende and wurtzite structural modifications. Thus, one cannot straightforwardly transfer the models developed for zinc-blende GaInN to the wurtzite polytype: an appropriate model should explicitly account for the particular structure type.

The second factor that can influence the modes of phase transformation in GaInN and should be explicitly taken into account in theoretical models is the elastic strain. The strains can arise in GaInN samples both due to local compositional fluctuations of Ga and In atoms, having noticeably different covalent radii, and, more globally, due to the fact that samples of GaInN are typically grown on substrates with noticeably different lattice parameters. For example, according to Refs. 4, 22, 28, and 29, sufficiently high biaxial compression associated with the growth of GaInN on a massive GaN substrate can completely suppress the trend to phase separation.

Also, in order to give reliable predictions concerning the particular decomposition modes in GaInN, a theoretical model should use adequate estimates for the material-dependent parameters (such as interatomic interaction energies), which are usually not identifiable experimentally. As shown in this work, quite moderate variations of these parameters can result in completely different decomposition modes. Only recently, there have appeared the treatments of InGaN decomposition (in both zinc-blende[23,29] and wurtzite[30] modifications), where the relevant parameters were estimated using sufficiently accurate first-principles calculations for different local atomic configurations of the alloy.

Finally, an essential limitation of practically all the existing theories is the adherence to thermodynamic approaches, where the main efforts are devoted to the adequate representation of the equilibrium free energy. In a quite sophisticated treatment of this kind,[29] the energies of several thousands of different ordering patterns in zinc-blende GaInN were estimated numerically by first-principles calculations in order to select the most energetically favorable ones. However, there is no guarantee that these most favorable configurations will be observed in practice. Indeed, at sufficiently high temperatures, phase transformations are suppressed by entropy contributions to the free energy, while at too low temperatures, they may require an unreasonably long time to form due to the suppressed atomic mobility. As a result, phase transformations can be observed only if the annealing temperature falls into the window between these regimes, which, depending on the properties of the particular material, can, but not have to, exist. In order to be quantitatively predictive, the theoretical approach should combine purely energetic calculations with kinetic methods. A good example is the above-mentioned Ref. 29, where the stability of the predicted ordered configuration in zinc-blende GaInN was checked against temperature variation using the Monte Carlo method.

In this work, we have investigated the minor component ordering in wurtzite $Ga_{1-x}In_xN$ ($x<0.5$) alloys using the kinetic rather than thermodynamic approach. First of all, using the total-energy density-functional calculations, we have determined the metal atom interaction parameters in $Ga_{1-x}In_xN$ and have checked their sensitivity to variations of alloy composition x and to external elastic strains. Second, instead of generating multiple ordered configurations of the alloys and comparing their energies, we have directly simulated the kinetics of the random alloy decomposition by lattice kinetic Monte Carlo (LKMC). With the help of such multiscale modeling, we have demonstrated not only the decomposition patterns corresponding to the *ab initio* values of metal atom parameters, but have predicted also how these patterns would be modified, provided these parameters were varied within reasonable limits.

II. COMPUTATIONAL DETAILS

In the current study, we investigate the possible modes of GaInN decomposition in a way, somewhat resembling the typical experimental approach. Namely, we select possible parameters of interatomic interaction (estimating them, in particular, by first-principles calculations) and perform computer "annealing" of initially random alloys, looking for the metal distribution patterns that evolve as a result. The kinetic description of the GaInN decomposition is performed in the standard "pseudobinary" approximation, because the probability of metal atoms to occupy the sites on nitrogen sublattice and vice versa is negligible. Correspondingly, only the metal atom redistribution on the hcp cation sublattice has been simulated by LKMC. The sizes of simulation cells varied from $\sim$16 500 to $\sim$33 000 of atomic sites on the metal sublattice, and the boundary conditions were periodic in all three principal directions.

The movement of atoms on the metal sublattice of GaInN results from the cation vacancy diffusion. The frequencies of individual vacancy jumps are given by the standard Gibbs relation

$$P^{\alpha} = \nu_0 \exp[-(E^{\alpha}_{sp} - E_{in})/k_B T], \tag{1}$$

where α is the index of the considered jump, ν_0 is an attempt frequency ($\sim 10^{13}$ Hz), E^{α}_{sp} and E_{in} are the energies of the crystal in the saddle point of the vacancy jump and in the equilibrium position prior to the jump, respectively, k_B is the Boltzmann factor, and T is the absolute temperature.

The saddle point energy for a vacancy jump was approximated in our simulations as $E_{sp}=E_m+\max(E_{in},E_{fi})$, where E_{fi} is the equilibrium crystal energy after the jump and E_m is the migration barrier, which in the simplest case is assumed to depend only on the chemical nature of the atom exchanging with the vacancy. In terms of this approximation, often referred to as Metropolis algorithm,[31] the vacancy jump probability is finally defined as

$$P^{\alpha} = \nu_0 \exp(-E^{\alpha}_m/k_B T) \times \begin{cases} \exp[(E_{in} - E_{fi})/\ k_B T) & \text{if } E_{in} < E_{fi} \\ 1 & \text{otherwise.} \end{cases} \tag{2}$$

For typical LKMC simulation cells of tens to hundreds of thousands of lattice sites, it is impossible to calculate directly the equilibrium energies of all possible configurations and so some approximations are normally used. Here, we restricted ourselves to the "pair-bond" approximation, where the energy of the crystal, E_{tot}, is represented as a sum of the energies e_{ij} of pairwise interactions (bonds) between individual atomic species on all lattice sites,

$$E_{tot} = \sum_i \sum_{j>i} e_{ij}(\mathbf{R}_i, \mathrm{A}_i; \mathbf{R}_j, \mathrm{A}_j), \tag{3}$$

where $\mathbf{R}_i$ is the lattice position of site i, and A_i, the type of the atomic species located on it. In our case, the possible atomic species include metal atoms (Ga and In) and vacancies (V) on the metal sublattice. It should not be forgotten that in such an approach, the "bonds" are virtual objects, rather than the real covalent bonds between atoms. The metal atoms in GaInN are too far away from each other and their interaction is mediated by nitrogen atoms.

According to the definition, the bond energies depend only on the chemical nature of species A_i and A_j terminating a bond and on the relative positioning of these species. Usually, the interaction between atoms in solids is short ranged and, hence, we can safely assume that e_{ij} is nonvanishing only for atomic pairs separated by a limited number K of nearest-neighbor distances. Then Eq. (3) can be rewritten as

$$E_{tot} = \sum_k^K \sum_{\mathrm{A,B}} n(\mathrm{A,B},k) e(\mathrm{A,B},k), \tag{4}$$

where $e(\mathrm{A,B},k)$ is the contribution to the total energy from a pair of atomic species A and B at the kth nearest-neighbor separation, and $n(\mathrm{A,B},k)$ is the total number of such pairs in the simulated crystal. In this study, we restrict ourselves to the first four nearest-neighbor distances, which correspond to metal pair configurations O-1ac (referred to below as 1NN or *ac* configuration), O-1a (2NN or *aa*), O-2ac (3NN or *ac*2), and O-2c (4NN or *cc*), as shown in Fig. 1.

Equation (4) can be somewhat simplified if we take into account an additional geometrical restriction,

$$\sum_{\mathrm{B}} n(\mathrm{A,B},k) = Z(k) N_{\mathrm{A}}/2,$$

where $Z(k)$ is the number of lattice sites in the kth coordination shell and N_{A} the total number of A-type atoms. Let us assume that we know the energy E_0 of some particular configurations of the considered system, where the numbers of bonds are $n_0(\mathrm{A,B},k)$. Let us also fix one of the available atomic species, C (as explained below, it pays off to select for C the majority component, in our particular case, Ga, because we restrict ourselves to alloys $\mathrm{Ga}_{1-x}\mathrm{In}_x\mathrm{N}$ with $x \leqslant 0.5$). Then Eq. (4) is easily reduced to

$$E_{tot} = E_0 + \sum_k^K \sum_{\mathrm{A,B}\neq\mathrm{C}} m(\mathrm{A,B},k) E_b(\mathrm{A,B},k|C), \tag{5}$$

where $m(\mathrm{A,B},k)=n(\mathrm{A,B},k)-n_0(\mathrm{A,B},k)$ and

$$E_b(\mathrm{A,B},k|C) = e(\mathrm{A,C},k) + e(\mathrm{B,C},k) - e(\mathrm{A,B},k) - e(\mathrm{C,C},k). \tag{6}$$

Presentation of the total energy in the form of Eq. (5) is especially convenient for LKMC simulations. First of all, it is easily seen that the energy change $E_{fi}-E_{in}$ in Eq. (2) is insensitive to E_0 and depends only on the bond energy combinations E_b. Second, the sum over components in Eq. (5) does not contain summation over C, so that atomic species of C type can be considered as a "background." Finally, where C is the majority component, E_b has a simple physical meaning, being essentially the binding energy of two nearby atomic species in a "monatomic" material C (in our case, pure GaN). For LKMC simulations, these binding energies are external input parameters that ultimately justify the interpretation of the simulated alloy kinetics as corresponding to a particular material.

Hence, for LKMC simulation of In redistribution in GaN matrix, we need three binding energies $E_b(\mathrm{In,In},k)$, $E_b(\mathrm{In,V},k)$, and $E_b(\mathrm{V,V},k)$ for each of the four considered interatomic separations k. The required binding energies were determined in this study as

$$E_b(\mathrm{A,B},k) = E_t(\mathrm{A,B},k) + E_{bulk} - E_t(\mathrm{A}) - E_t(\mathrm{B}), \tag{7}$$

where E_{bulk}, $E_t(\mathrm{A})$, and $E_t(\mathrm{A,B},k)$ are the total energies of identical GaN supercells containing, respectively, no extra atoms, one atom of type A, and an atomic pair (A,B) at separation k. The calculations of these total energies were performed using the density-functional-theory-based code[32] VASP with the local density approximation.[33] The interaction between ions and electrons was described using the projector-augmented wave method,[34] treating $3d$ electrons of gallium and $4d$ electrons of indium as valence states. The considered simulation supercells for wurtzite GaInN contained from 4 to 300 atoms, depending on the particular task pursued. Periodic boundary conditions were used. The reciprocal space integrals were approximated by sums over from (9,9,9) to (1,1,1) Monkhorst-Pack special points (depending

on the supercell size), folded within the irreducible part of the Brillouin zone.[35]

According to these *ab initio* calculations, cation vacancies in GaN interact neither between themselves nor with In atoms, i.e., $E_b(\mathrm{In},\mathrm{V},k)=E_b(\mathrm{V},\mathrm{V},k)=0$. In other words, the only role of cation vacancies in GaN is to enable the jumps of In atoms. Hence, in our simulations, only one vacancy per cell was considered, which, having in mind periodic boundary conditions, corresponded to vacancy concentrations of $\sim(3-5)\times 10^{-5}$. The fact that vacancy concentration in real samples can be even lower does not affect the simulation output, but increases the time scale, because at very low vacancy concentration, any piece of the sample with the volume of LKMC simulation cell remains, for most of the time, devoid of any vacancies. Since, in this paper, we are interested mostly in the qualitative behavior of decomposing GaInN, and not so much in particular time scales, we circumvent below the problem of vacancy concentration, characterizing the kinetics not in terms of the elapsed time (though it is also estimated by the employed code CASINO-LKMC), but in terms of the number of performed Monte Carlo steps or, equivalently, vacancy jumps [in the algorithm employed, each Monte Carlo step corresponds to one vacancy jump]. For the same reason, in some calculations, we did not consider vacancies at all, allowing In atoms to directly exchange places with the first nearest-neighbor (1NN) Ga atoms on the metallic sublattice. This simplification allowed us to noticeably accelerate the annealing kinetics, especially at low In contents. The acceleration is achieved, naturally, at the expense of losing the correlation effects in In self-diffusion, but several parallel runs, where the diffusion was either mediated by a vacancy or performed via the direct In-Ga exchange, demonstrated no difference in the resulting decomposition patterns.

III. RESULTS AND DISCUSSION

As is well known from the theory of alloys,[26] the outcome of alloy decomposition is determined by the competition of the energy and the entropy contributions to the alloy free energy. For this reason, the decomposition trends are most pronounced at low temperatures, where the energy contribution dominates. Correspondingly, if pairing together two separated In atoms gives a gain in the total crystal energy, one can expect that the InN/GaN phase separation would dominate at sufficiently low temperatures. Assuming that the total crystal energy is reasonably well represented by Eq. (5) and having in mind that the elastic interaction of atoms in covalent crystals is relatively short ranged, one can make rough qualitative conclusions concerning the alloy decomposition trends based on the binding energies of the simplest clusters (atomic pairs) in very diluted alloys. Correspondingly, we have started with the first-principles calculation of the energies of a number of In atom configurations corresponding to low In contents in the alloy.

First of all, we have estimated the equilibrium cell sizes corresponding to different In concentrations in the matrix (= different numbers of In atoms randomly distributed in the *ab initio* simulation cell). This was necessary in order to correctly account for changes in the lattice parameters of the alloy, a and c, caused by the noticeable difference of Ga and In covalent radii. For pure GaN, the obtained value of $a=3.153$ Å is somewhat lower than the experimental one [3.19 Å (Ref. 27)], but the obtained c/a ratio is very close to the experimental one (1.632 vs 1.626, respectively). Having in mind that the ratio c/a varies with the change of In content only a little [slightly decreasing from 1.626 in GaN to 1.62 in InN (Ref. 27)], the energies of supercells with different amounts of In atoms were minimized only with respect to a, keeping the ratio c/a fixed at the value obtained for GaN (Fig. 2). The resulting equilibrium values of a increase linearly as a function of In content x in the alloy $Ga_{1-x}In_xN$ and the slope of 0.34 Å practically coincides with the experimental estimate.

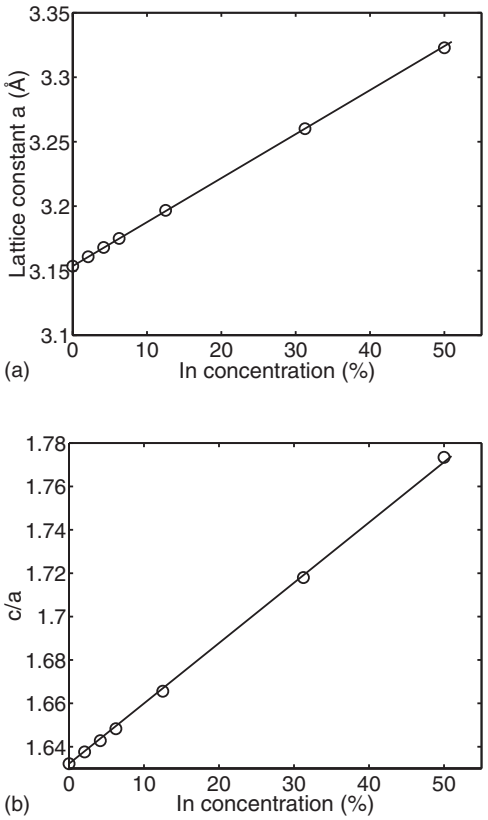

FIG. 2. (a) The dependence of the basal lattice parameter a on In content in the alloy $Ga_{1-x}In_xN$ (c/a fixed at 1.632). (b) The variation of equilibrium c/a ratio as a function of In content in a cell with parameter a fixed at a value corresponding to pure GaN.

Then it has been checked how the nonrandomness in the spatial distribution of In atoms affects the energy of the system. For that purpose, we have calculated the total energies of *ab initio* supercells containing several differently disposed pairs and trios of In atoms. In each case, one configuration (indicated as a random one) was selected so as to provide the biggest possible distances between In atoms in a supercell (taking into account the periodic boundary conditions). In order to eliminate the effect of lattice expansion due to the addition of In atoms, the lattice parameter a in each case was allowed to fully relax. The calculated results are summarized in Table I. For comparison purposes, Table I contains also the

TABLE I. The energies of 96-atom *ab initio* supercells with different numbers and configurations of In atoms.

In atoms	Configuration	x	E_{tot} (eV)	E_g (eV)	E_b (eV)
0		0	−669.31		
1		0.021	−667.34		
2	*aa*	0.042	−665.30	−0.11	−0.07
2	*ac*	0.042	−665.37	−0.04	0.00
2	*ac*2	0.042	−665.42	0.01	0.05
2	*cc*	0.042	−665.52	0.11	0.15
2	Random	0.042	−665.41		0.04
3	*aaa*	0.063	−663.23	−0.30	−0.17
3	*aca*	0.063	−663.54	0.01	0.14
3	Random	0.063	−663.53		0.13

total energies for pure GaN cell and for a cell with one In atom. As can be seen, a nearby location of In atoms changes the supercell energy as compared to the random atomic disposition, and some configurations are energetically more favorable than the random distribution of In atoms (as indicated by the positive energy gain E_g, calculated as the energy difference between the random dispositions of In atoms and their close configurations at the same number of In atoms in the supercell; see Table I). It is seen, in particular, that indium atom disposition along [0001] direction is energetically favorable, but not in the basal plane. Both these conclusions are in agreement with the earlier analytical predictions employing electrostatic dipole energy calculations.[36]

The gain energies E_g in Table I cannot, unfortunately, be directly associated with the binding energies of In pairs, as defined by Eq. (7), for at least two reasons. First of all, the computational cell for each configuration was fully relaxed and, hence, corresponded to slightly different cell sizes. Though very small (within 2×10^{-4} Å), this difference can still modify, in an unpredictable way, the gain energy, which is in itself a very small difference of the total cell energies. Second, the computational cell size used (96 atoms) is too small to completely exclude the interaction of indium atoms with their periodic images, and, hence, the "random" configurations above may not be a good reference at all. The second drawback can, however, be overcome if we calculate the binding energy of an arbitrary configuration X of In atoms as

$$E_b(\mathrm{X}) = mE_{tot}(1) - (m-1)E_{tot}(0) - E_{tot}(\mathrm{X}), \tag{8}$$

where $E_{tot}(0)$ and $E_{tot}(1)$ are the total energies of the pure GaN cell and the cell with one In atom, while m (=2 or 3) is the number of In atoms in the simulation cell. The binding energies thus obtained can, in contrast to E_g, be interpreted as the "strain-free" values, because all total energies in Table I correspond to strain-free supercells. Note, however, that Eq. (8), when applied to random configurations, gives nonzero binding energies, which should not be the case for truly noninteracting atomic configurations.

The comparison of the obtained binding energies for trios of In atoms with those for In pairs indicates that the "bond" model, as described by Eq. (4), is indeed a reasonable approximation, because the energies of both *aaa* and *aca* chains are reasonably close to the sums of pairwise energies relevant to each configuration.

Judging from the calculated gain energies, we can expect that clustering of In atoms in the basal plane [at second nearest-neighbor (2NN) distances] is suppressed. On the other hand, the energy gain accompanying In atom accommodation along [0001] should prompt the formation of In atom chains in the c direction. Though the binding energy between In atoms in configuration *cc* is not high, it allows clustering at least at low temperatures, where the temperature-induced disordering is weak. LKMC simulation performed with the above-cited energy gains, taken at their face value, demonstrates that this ordering pattern should indeed be the dominant trend in low-In alloys [Fig. 3(a)].

At this junction, it is worth mentioning that the prediction of the ordering and/or decomposition patterns in GaInN based on the defect binding energies, even calculated by first-principles approach, remains rather uncertain. First of all, this is related to the fact that the interaction energies

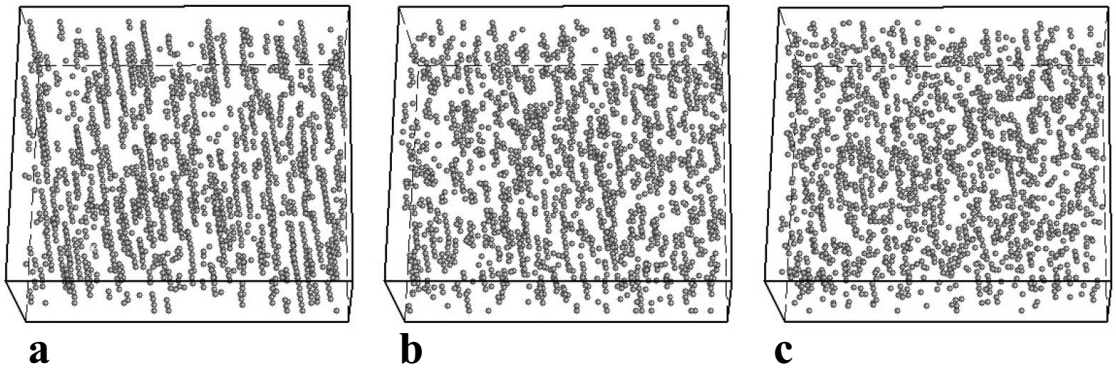

FIG. 3. Typical patterns of In atom distribution in LKMC simulation cell after annealing of $Ga_{0.9}In_{0.1}N$ alloy at (a) 473 K, (b) 673 K, and (c) 873 K, assuming the energy gains for local short range ordering as given in Table I. Only In atoms are shown. The indium atomic chains, especially at higher temperatures, are in dynamic equilibrium, being continuously destroyed and recreated. The equilibrium is achieved well within 1 million vacancy jumps, which, assuming vacancy concentration of 6×10^{-5} (one vacancy per simulation cell) and migration energy of 1.6 eV (Ref. 37), corresponds to times of ~100 years, 2.4 h, and 15 s for cases (a), (b), and (c), respectively.

between metal atoms are quite low, regardless of the difference in the covalent radii of In and Ga (~11%). The reason is that Ga and In atoms on the metallic sublattice do not interact directly. As shown by our estimates, Ga atoms closest to a sole In atom shift from their site positions by less than 0.06 Å (<2% of Ga-Ga separation), while all the differences in covalent radii are compensated by shifts of intervening nitrogen atoms (Fig. 4). Because of the generally low interaction energy values, relatively small changes of them (related, e.g., to the binding energy estimation procedure) can lead to qualitatively different results. As a simple illustration, let us consider the formation of zigzag chains (that is, the chains aligned in the prismatic direction and consisting of a continuous repetition of *aca* configuration). With the current definition of the binding energies, two *c* chains shifted by one interatomic distance in the *ac* direction do not interact (see Table I) and zigzag chains formed accidentally by close pairs of *c* chains are observed in LKMC simulations rarely, but persistently. Replacement of the vanishing binding energy at the 1NN distance with a small negative value (as obtained for E_g in Table I) completely suppresses the formation of zigzag chains in LKMC simulations.

Second, the energy gains associated with the correlated disposition of indium atoms are not the only parameters that determine whether the alloy ordering or phase separation is observed in practice. No less important for the decomposition kinetics and outcome are the annealing temperature and the In content in the alloy.

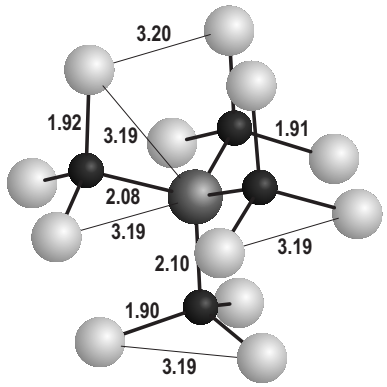

FIG. 4. The atomic relaxation pattern around an In atom in GaN (in 192-atom *ab initio* cell). For comparison, the calculated equilibrium Ga-N and Ga-Ga distances are 1.936 and 3.153 Å, respectively.

The annealing temperature affects the diffusion kinetics in two opposite ways. On the one hand, due to entropy considerations, the efficiency of clustering falls down with the increase of the annealing temperature [Figs. 3(b) and 3(c)]. On the other hand, the atomic mobility exponentially increases with the temperature increase. A possibility to observe the decomposition within the experimentally reasonable times (hours to days) arises only provided there exists a temperature region where a compromise between these two trends

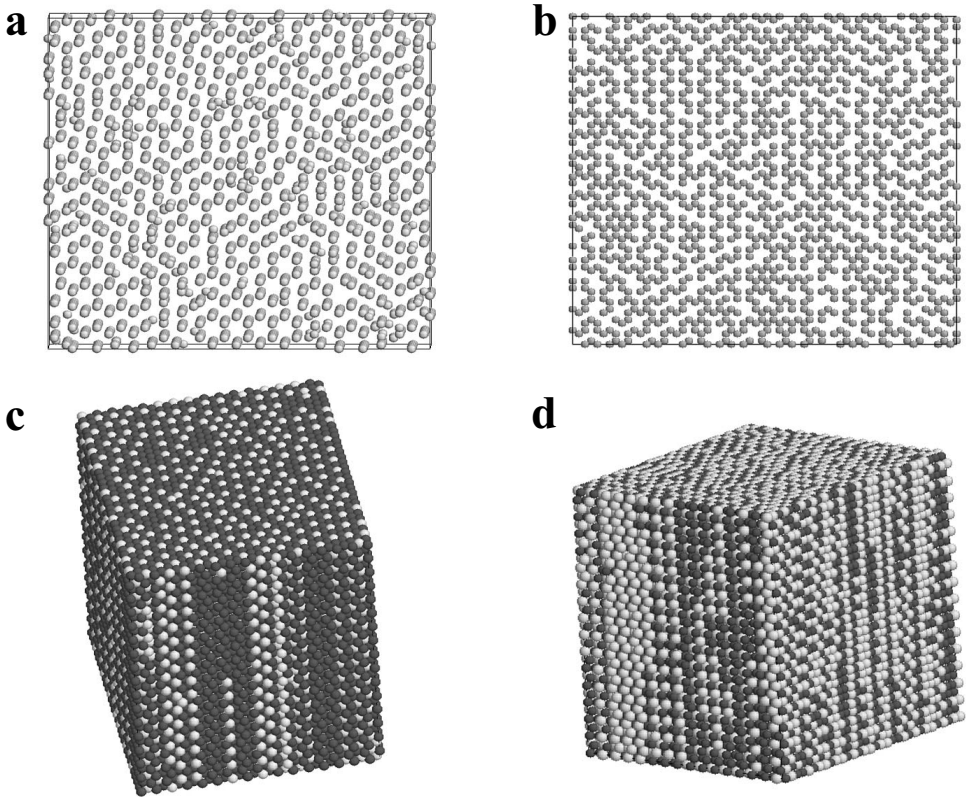

FIG. 5. The ordering patterns in $In_xGa_{1-x}N$ after annealing at 473 K. [(a) and (c)] $x=0.25$, duration: 30 million vacancy jumps. The set of In-In binding energies (in eV) at 1NN–4NN positions: (−0.11, −0.04, 0, and 0.11). [(b) and (d)] $x=0.5$, duration: 5 million vacancy jumps. In-In binding energies (in eV) set: (−0.11, −0.04, 0, and 0.11). White spheres in (c) and (d) and subsequent figures represent In atoms, while dark spheres represent Ga; nitrogen atoms are not shown. (a) and (b) show only In atoms viewed along ⟨0001⟩, while (c) and (d) are three-dimensional views of simulation cells with basal plane parallel to the top surface.

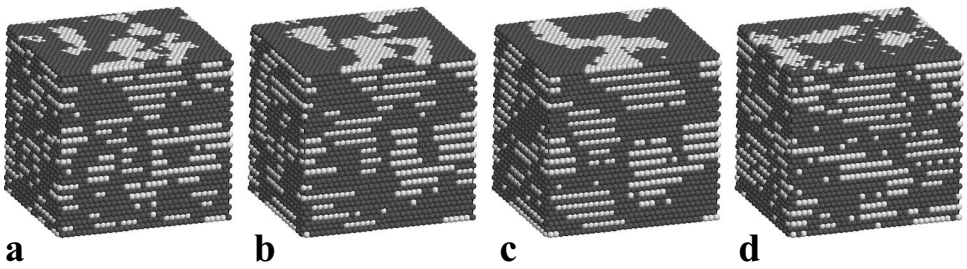

FIG. 6. The ordering patterns in $In_{0.25}Ga_{0.75}N$ annealed with the In-In binding energies (in eV) of (−0.08, 0.04, 0.01, and 015). [(a)–(c)] $T=273$ K, intermediate configuration of the same LKMC run at 6, 20, and 70 million vacancy jumps, respectively. (d) $T=473$ K, 20 million vacancy jumps.

can be achieved. For the used set of the binding energies, the ordering trend is hardly seen already at 673 K, while the time required to establish the dynamic equilibrium in the system remains reasonable only slightly below this temperature and, thus, the chances to observe the ordering for the gain parameters summarized in Table I are quite low, unless in a specially tailored experiment.

In nondilute $Ga_{1-x}In_xN$ alloys (with $x \geq 0.12$), the relative distribution of In atoms becomes sensitive, in addition to the energy gain reasons, to geometrical restrictions, which force some In atoms to occupy the energetically unfavorable places. It is practically impossible in this situation to predict *a priori* which decomposition pattern finally dominates. For example, the selection of In-In binding energy values as in column "E_g" results at $x=0.25$ in a columnar ordering of In atoms along the c axis [Figs. 5(a) and 5(b)], while selection of quite similar values from column "E_b" leads to no discernible ordering. On the contrary, the latter binding energies in LKMC simulations for $In_{0.5}Ga_{0.5}N$ lead to interpenetrating "walls" of In and Ga atoms, aligned along the c axis [Figs. 5(c) and 5(d)].

For alloys with low In content, it is practically impossible to correlate the LKMC predictions with the experimental observations. X-ray diffraction measurements discover no ordering at In contents below 0.2,[11] but, on the other hand, even very pronounced In chains, as shown in Fig. 3(a), practically do not modify the x-ray diffraction pattern. On the other hand, ordering is definitely predicted for $In_{0.5}Ga_{0.5}N$,[11] but the experimentally observed "1:1" ordering pattern (the interchange of basal planes filled with Ga and In) is equally definitely different from that shown in Fig. 5.

The simplest excuse would be to ascribe the experimentally observed phase decomposition patterns to some specific mechanisms that are active exclusively during the sample growth (e.g., ordering at the growing sample surface[14]). However, even if this was the case, it does not explain the observed InN precipitation during the high-temperature annealing.[7] It is not clear either why the 1:1 ordering, even if formed on the growing surface, would persist inside the film during quite long (~1 h) growth process at 700–800 °C (Ref. 11) if it is thermodynamically unfavorable. Hence, it makes sense to look for other possible reasons for the versatile phase decomposition patterns, not related to the peculiarities of the sample growth process.

The most relevant here seems to be the already mentioned fact that the values of the metal binding energies in GaInN, no matter how defined, are quite small. Correspondingly, relatively small variations of the binding energies are sufficient to cause sometimes (e.g., when the ratios of binding energies noticeably change or some binding energies change sign) a drastically different outcome of the alloy decomposition. Thus, Fig. 6 demonstrates that the modification of the energy of *aa* bond (from −0.4 to 0.4 eV) suffices to obtain the domains of 1:1 ordering. The decomposition into ordered regions of $Ga_{0.5}In_{0.5}N$ and regions of pure GaN at 273 K required less than 5×10^6 vacancy jumps in a crystal of $\sim3.3\times10^4$ cation sublattice sites. At higher annealing times, the ordered regions changed shape and tended to roughen [Figs. 6(a)–6(c)]. The increase of the annealing temperature to 473 K introduced bigger disorder, but the ordering pattern remained clearly discernible.

In order to better demonstrate the sensitivity of metal redistribution modes to the input parameters, we have performed a series of LKMC runs with different relations between the binding energies of close In-In pairs. In order to avoid uncertainties in the In-In binding energies related both to rather small size of the *ab initio* cells used for the estimates in Table I and to the independent relaxation of cells with different In-In pair configurations, these simulations were oriented at the self-consistent set of binding energies (see Table II), obtained for a 300-atom *ab initio* computational cell with the basal lattice parameter as in pure GaN and with c/a ratios as in either relaxed supercell or $Ga_{0.5}In_{0.5}N$. Only interaction energies corresponding to the first four nearest-neighbor separations between In atoms were considered, because at higher separations, the In-In interaction is negligible (the estimated binding energies at 5NN and 6NN separations were below 0.005 eV). In each LKMC run, one or two of these parameters were varied so as to

TABLE II. The binding energies of In-In atom pairs in 300-atom GaN calculation cell with lattice parameters of (a) relaxed GaN and (b) $Ga_{0.5}In_{0.5}N$ on thick GaN substrate.

Configuration	E_b (eV)	
	a	b
aa	−0.08	−0.04
ac	−0.067	−0.078
*ac*2	0.005	0.012
cc	0.04	0.02

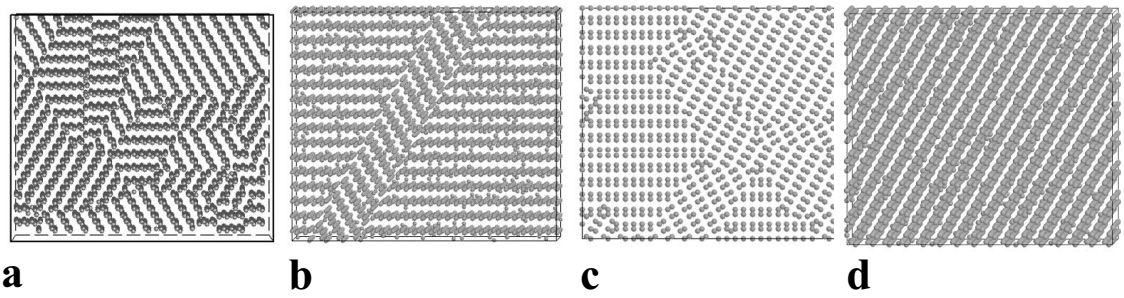

FIG. 7. Some *c*-aligned ordering patterns in LKMC-annealed $Ga_{0.5}In_{0.5}N$. [(a) and (b)] The In-In binding energy set of (−0.08, −0.04, −0.03, and 0.07 eV). Annealing (a) at 273 K for 2×10^6 direct In-Ga exchange jumps and (b) at 473 K for 4×10^6 direct In-Ga exchange jumps. [(c) and (d)] The In-In binding energy set of (−0.08, −0.04, 0.02, and 0.015 eV). Annealing (c) at 273 K for 2×10^6 direct In-Ga exchange jumps and (d) at 473 K for 3×10^6 direct In-Ga exchange jumps. In all figures, only In atoms are shown; the viewing axes are close to ⟨0001⟩.

check their effect on the resulting kinetics. We do not discuss at the moment the possible physical reasons for such parameter variations; this is postponed to the later part of the paper. The runs were deliberately performed at relatively low temperatures in order to minimize the disordering effects of the annealing temperature. The In content of 50% was selected on the assumption that this simple In:Ga ratio allows clear ordering patterns.

A variety of phase decomposition patterns in $Ga_{0.5}In_{0.5}N$ is demonstrated in Figs. 7–10. Selecting different binding energy sets, one can observe various types of ordering along the *c* axis (Fig. 7), 1:1 ordering (Figs. 8 and 9), and spinodal decomposition without any ordering (Fig. 10). In sufficiently big simulation cells, the formation of ordered domains is observed, the size of which typically grows with the increase of temperature. As could be expected, the ordering is very clear at low temperatures, but the increase of temperature decreases the ordering degree due to the increase of the mixing entropy contribution.

It is interesting to note that the 1:1 ordering in $Ga_{0.5}In_{0.5}N$ can be obtained for substantially different combinations of input parameters. The most obvious is, as in Fig. 6, a combination of the positive 2NN binding energy (in the basal plane) with sufficient repulsion at the 1NN distance [Figs. 8(a) and 8(b)]. A less evident possibility involves the only positive binding at the fourth nearest-neighbor (4NN) distance [Figs. 8(c) and 8(d)]. In the latter case, the crucial part is played by the repulsion of In atoms at the third nearest-neighbor (3NN) separation, its increase from −0.01 eV [as in Figs. 8(c) and 8(d)] to −0.02 eV results in the very pronounced and uniform ordering, as can be easily seen in Figs. 9(a) and 9(b). Even at a rather high temperature of 673 K, where the ordering in LKMC simulation cell is not easily detected when viewed along the basal plane, as in Figs. 9(a) and 9(b), a look along the *c* axis clearly demonstrates that only separate In atoms are captured in the Ga planes [Fig. 9(c)]. In contrast, phase separation in the form of spinodal decomposition (Fig. 10) requires that both 1NN and 2NN pairs have positive binding energies.

We, thus, see that practically all the experimentally observed modes of phase decomposition, in addition to those not observed experimentally in GaInN, can be reproduced with the parameters not much different from those summarized in Tables I and II. The question is, however, why the *ab initio* predictions fail to fall in the range compatible with the experimentally observed patterns. Below we discuss some possible reasons for that, deliberately putting aside those that we are unable to verify [e.g., that the experimentally observed 1:1 ordering is due purely to the film surface growth peculiarities and would never arise during the annealing of a random alloy, or that density-functional theory, which is, after all, an approximate method, unexpectedly fails in the case of GaInN].

The first reasonable possibility is related to the action of high elastic strains in GaInN samples. The experimentally observed decomposition occurs in GaInN layers grown on substrates with much smaller lattice parameter (typically, GaN) and, thus, are strongly anisotropically strained. As al-

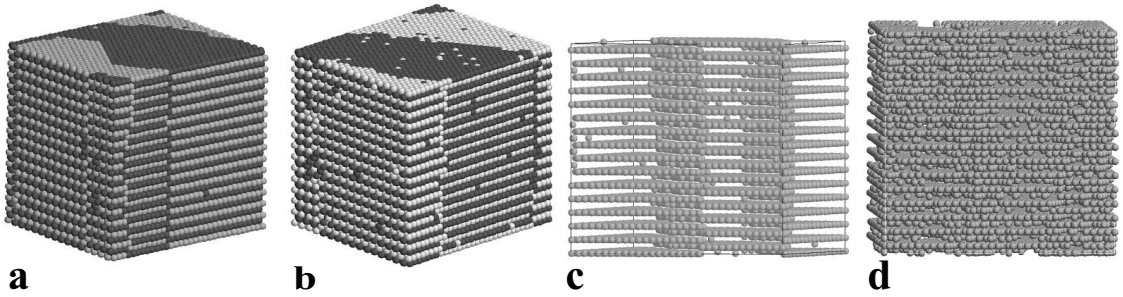

FIG. 8. Examples of 1:1 ordering patterns in LKMC-annealed $Ga_{0.5}In_{0.5}N$. [(a) and (b)] The In-In binding energy set of (−0.08, 0.04, 0.03, and 015 eV). Annealing for 1.5×10^7 vacancy jumps at (a) 473 K and (b) 673 K. [(c) and (d)] The In-In binding energy set of (−0.08, −0.04, −0.01, and 0.015 eV) only In atoms are shown. Annealing for 2×10^6 direct In-Ga exchange jumps at (c) 273 K and (d) 473 K.

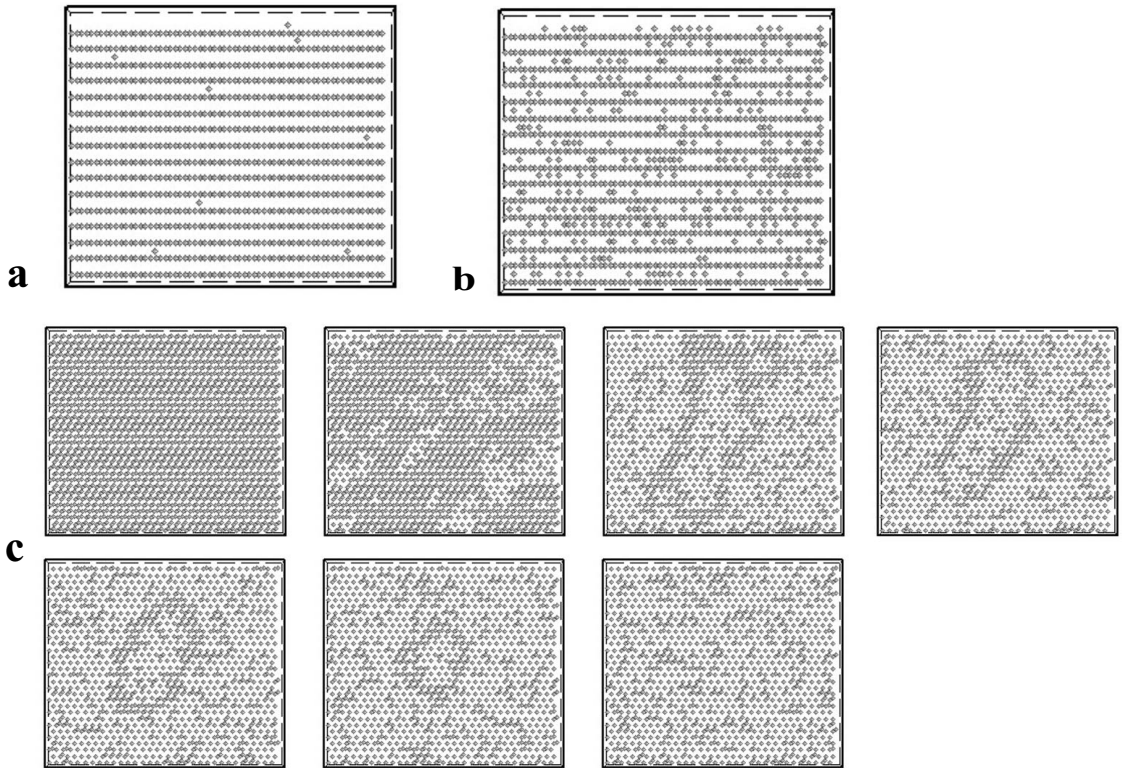

FIG. 9. Clearly pronounced 1:1 ordering patterns in LKMC-annealed $Ga_{0.5}In_{0.5}N$ with the In-In binding energy set of (−0.08, −0.04, −0.02 and −0.015 eV). Annealing for 10^6 direct In-Ga exchange jumps at (a) 273 K and (b) 473 K, viewed parallel to basal planes. (c) A sequence of annealing steps of the same run (from 0 to 6×10^6 direct In-Ga exchange jumps with the interval of 10^6 jumps) at 673 K, viewed along the *c* axis. The loop at intermediate annealing steps is a domain boundary.

ready mentioned in the Introduction, the fact that high biaxial compression affects both phase precipitation and ordering (suppressing the former, but promoting the latter) is supported by experimental evidences[4] and previous *ab initio* calculations (for zinc-blende GaInN).[22,29] Earlier, we demonstrated that for some semiconductor systems [e.g., Si (Ref. 38) or SiGe (Ref. 39)], high elastic strains were able to strongly affect the relations between the binding energies

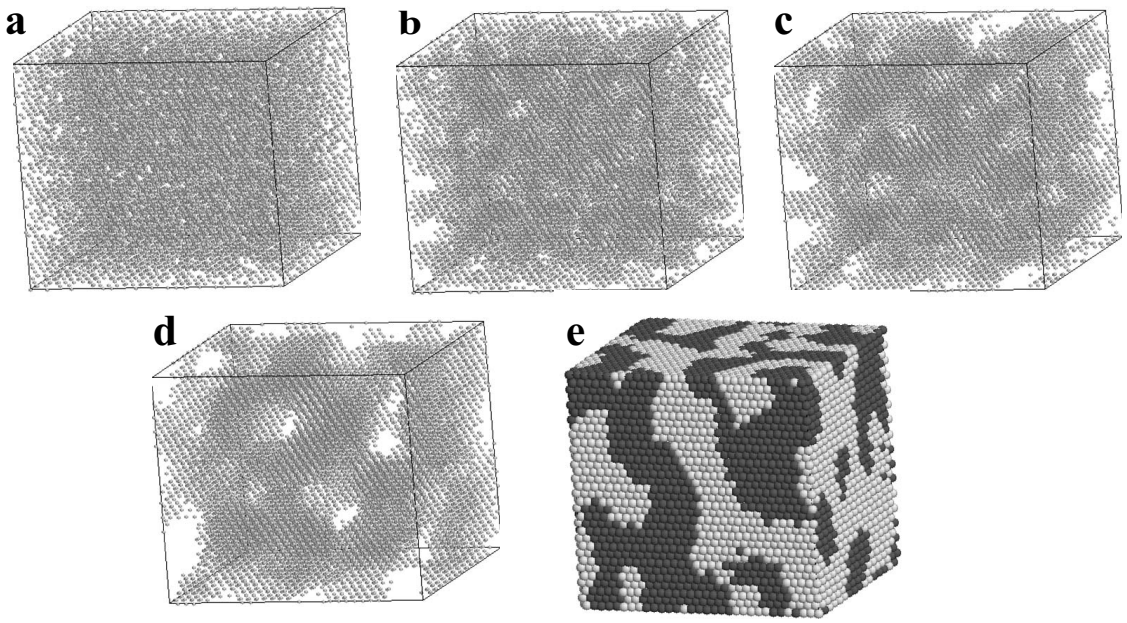

FIG. 10. Spinodal decomposition in $Ga_{0.5}In_{0.5}N$ during the LKMC annealing run at 473 K. The In-In binding energy set: (0.08, 0.04, −0.01, and −0.015 eV). (a)–(d) show the spatial distributions of In atoms after (0, 1, 10, and 100) $\times10^6$ vacancy jumps. (e) shows the distribution of both Ga (dark) and In (light) atoms in LKMC simulation cell after 9×10^7 vacancy jumps.

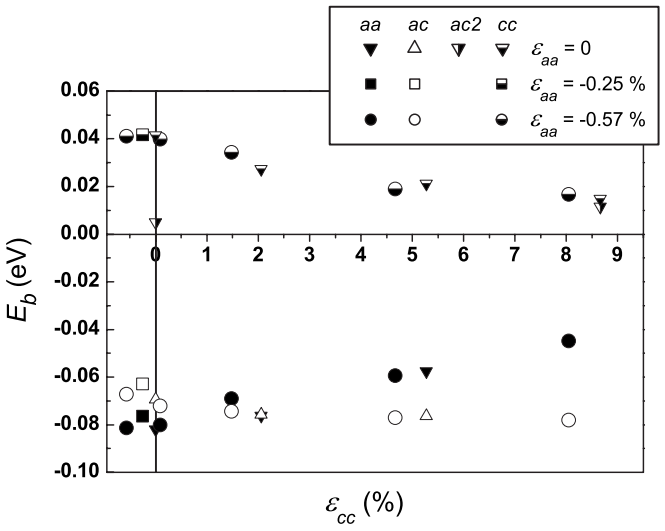

FIG. 11. The binding energies of four In-In pair configurations at different biaxial strains.

between atom pairs at different interatomic separations. Hence, we have studied whether the biaxial compression arising in GaInN films growing on a standard GaN substrate was sufficient to modify the binding between In atoms in a way required to observe the experimental ordering patterns.

In order to estimate the effect of biaxial strains on the binding energies of In atoms, we have calculated by *ab initio* the total energies of supercells with different lattice parameters. In order to minimize the effect of image interaction, 300-atom monoclinic cells (with $5\times5\times3$ elementary wurtzite cells) were used. In the calculations, we varied independently both the in-plane parameter a (from the obtained equilibrium value for pure GaN, 3.135 Å, up to 3.153 Å) and the ratio c/a (from 1.63 to 1.77). For each combination of the lattice parameters, the total energies for six supercells (that is, pure GaN cell, a cell with one substitutional In atom, and four cells with two substitutional In atoms at separations from 1NN to 4 NN) have been calculated.

From these data sets, the binding energies of In atoms at different separations have been estimated according to Eq. (5). The resulting binding energies at different strains (calculated with respect to pure GaN as a reference state) are shown in Fig. 11. It can be seen that the binding energies are quite sensitive to straining in the prism direction, but much less so for the in-plane compression [in fact, the data for different considered in-plane strains ε_{aa} fall practically on the same trend lines (Fig. 11)]. Two features of the results presented in Fig. 11 are worth mentioning. First of all, quite noticeable differences to the results in Table I can be observed. In particular, much weaker binding at the 4NN separation is obtained, while the lacking interaction at the 1NN separation is replaced with quite noticeable repulsion. On the other hand, the repulsive in-plane interaction is affected to a very minor degree. Second, the expansion in prismatic direction changes at least two of the binding energies quite noticeably. However, all of them remain small and neither changes the sign.

In order to estimate the effect of biaxial strain variations on the ordering, a series of LKMC runs has been executed for alloys with different In contents x, assuming that the biaxial strains in them correspond to the growth of $Ga_{1-x}In_xN$ alloy on a thick GaN substrate. In these calculations, the binding energies of In atom pairs were assumed to be insensitive to the particular chemical environment around the pairs (as appropriate for the pair-bond model), which allowed us to apply the bond energy variation with strain, shown in Fig. 11, to alloys with variable In content. The in-plane and prismatic strains, corresponding to alloy $Ga_{1-x}In_xN$, are defined as

$$\varepsilon_{aa}=[a-a_0(x)]/a_0(x) \quad \text{and} \quad \varepsilon_{cc}=[c-c_0(x)]/c_0(x),$$

where a, c are the actual lattice parameters and $a_0(x)$, $c_0(x)$ the equilibrium lattice parameters for the alloy with indium content x. As assumed above, a in all cases remains that of pure GaN, while c varies according to the loading conditions in prismatic direction. Assuming after the experiments that the complete stress relaxation in the c direction is allowed, the variation of c in a random alloy has been calculated as a function of x, as shown in Fig. 2(b). The equilibrium in-plane lattice parameter $a_0(x)$ was taken for each considered In content as in Fig. 2(a), while $c_0(x)$ was recalculated from $a_0(x)$ using the relation $c_0=1.632a_0$. The resulting strains and corresponding binding energies (as extrapolated from trend lines in Fig. 11) are collected in Table III.

The alloy decomposition modes, corresponding to the sets of binding energies collected in Table III, were determined using LKMC simulation of the annealing of initially random alloys $Ga_{1-x}In_xN$ with different In contents. The annealing temperature was deliberately kept quite low (273 K) in order to clearly reveal the ordering pattern, if any. The simulations at In content of 10 at. % has demonstrated no stable ordering picture, even though small transient regions of local order

TABLE III. The external strains and the binding energies of In pairs at different separations, estimated from the *ab initio* calculations.

In content (at. %)	ε_{aa} (%)	ε_{cc} (%)	$E_b(aa)$ (eV)	$E_b(ac)$ (eV)	$E_b(ac2)$ (eV)	$E_b(cc)$ (eV)
0	0	0	−0.08	−0.072	0.005	0.04
10	−1.07	2	−0.065	−0.078	0.007	0.03
25	−2.6	4.3	−0.06	−0.08	0.008	0.02
37.5	−5.1	6.5	−0.05	−0.08	0.01	0.015
50	−9.7	8.7	−0.04	−0.08	0.012	0.015

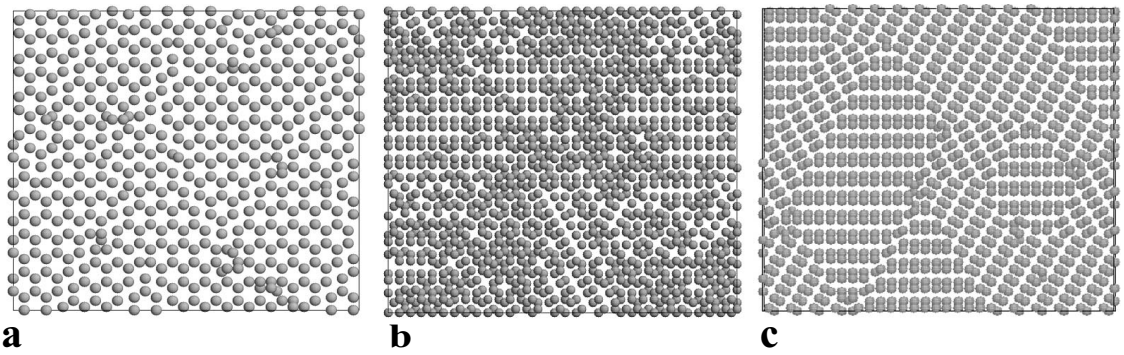

FIG. 12. The ordering patterns predicted by LKMC as a result of annealing at 273 K. (a) $x=0.25$, 6×10^6 In jumps; (b) $x=0.375$, 9×10^6 In jumps; (c) $x=0.5$, 3×10^6 In jumps. In all cases, the view is along the c axis.

could be detected from time to time. On the contrary, at $x \geqslant 0.25$, the ordering is quite pronounced, though the mode depends on the indium content (see Fig. 12). In all cases, the domain structure was formed. With the increase of the annealing temperature, the domain size increases, but the amount of In atoms in disordered positions increases as well. Nonetheless, at $x=0.25$ and 0.5, where the In content fits the value required for the perfect pattern, the ordering remains clearly detectable even when the annealing temperature is increased to 673 K, which would provide sufficient vacancy mobility to allow the experimental observations.

For all considered In contents, the ordering demonstrates alignment along the c axis rather than the experimentally observed 1:1 pattern. In fact, this could be expected, because the bond energies for all x in Table III favor neither *aa* nor *ac* close pairs of the like atoms. This means that the effect of elastic strains is by itself insufficient to modify the *ab initio* values to the necessary degree and some different reasons to reconcile the modeling with the experiment are to be found.

The fault can be, for instance, in the scheme that we use to extract bond energies from first-principles calculations. Indeed, above we assumed that the average effect of various chemical compositions around a close In-In pair can be fully reproduced in terms of the average strain acting on the same bond embedded in a purely GaN matrix. Though it is reasonable to expect that this approach works nicely at low indium contents, there is no guarantee that it is equally good for concentrated alloys. In order to check this possibility, we have calculated the energies of several random distributions of Ga and In atoms over lattice sites for an alloy with composition $Ga_{0.5}In_{0.5}N$. The lattice parameters of the supercell were selected as appropriate for this composition [see Fig. 2(a)]. The binding energies were then found by the least squares fit. The resulting values are summarized in Table IV; the differences between the total energies calculated by *ab initio* and those estimated by Eq. (5) with the fitted values were below 0.025 eV. As can be seen, the signs of binding energies are exactly reversed as compared to those for In pairs on GaN lattice. Correspondingly, the alloy decomposition pattern simulated by LKMC (Fig. 13) shows ordering mostly in the basal plane, but quite different from 1:1. Following the same terminology, it is better described as "2:2." Similar to the results presented above, ordering is observed only in the limited temperature range (practically no discernible ordering is seen already at 673 K [Fig. 13(c)]) and the decomposition into domains is quite pronounced (the domain size in the basal plane decreasing with the decrease of temperature).

TABLE IV. The binding energies found by the least squares fit to the *ab initio* total energies for several random distributions of In and Ga atoms over supercell sites in $Ga_{0.5}In_{0.5}N$.

Configuration	E_b (eV)
aa	0.024
ac	0.028
*ac*2	−0.027
cc	−0.064

Unfortunately, the decomposition pattern shown in Fig. 13 cannot be definitely preferred to the other possibilities discussed above, because the confidentiality limits for the least squares fit are a few hundredths of eV. Though not big in themselves, they exceed in the absolute value the parameters cited in Table IV and, hence, tolerate quite arbitrary changes of bond energy signs, with all the accompanying consequences. This seems to be, in fact, the main difficulty for LKMC simulations of phase decomposition in GaInN: the absolute values of the relevant parameters are very small and their variations in quite reasonable limits (in order to answer both the differences in experimental conditions and the model uncertainties) are able to drastically modify the simulation output. On the other hand, the same may be the reason for the experimentally observed versatility of phase decomposition patterns in GaInN and their sensitivity to the particular experimental conditions.

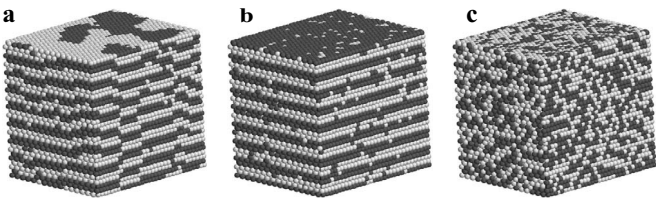

FIG. 13. The patterns predicted by LKMC as a result of annealing of initially random $Ga_{0.5}In_{0.5}N$ with the input parameters summarized in Table IV. (a) 273 K, 1.8×10^7 vacancy jumps; (b) 473 K, 2×10^8 vacancy jumps; (c) 673 K, 10^7 vacancy jumps.

A possible way to improve the reliability of the modeling predictions can be to proceed beyond the pairwise description of metal atom interactions and replace Eq. (4) with a more detailed Hamiltonian. One such possibility is proposed in Ref. 19, where the pairwise interaction term in the total crystal energy was supplemented with the contribution describing the "tetrahedral" correlation in the spatial distribution of metal atoms connected to the same nitrogen atom. Indeed, the interactions of metal atoms in the real alloy are mediated by intervening nitrogen and, hence, not only the stretching of metal-nitrogen bonds, but the changes in dihedral angles between them can give non-negligible contributions to the total crystal energy. However, the further improvements of the model are beyond the scope of this paper.

IV. CONCLUSIONS

Summing up, our simulations demonstrate that the phase decomposition patterns in wurtzite GaInN are very sensitive to the interplay of metal atom interactions at several interatomic distances (at least to the fourth nearest neighbors) on the cation sublattice.

Several approaches used to estimate the corresponding interaction energies from the accurate first-principles calculations agree in that the differences between these energies are quite small, but the absolute values and, even more importantly, the signs of the binding energies of In atoms turn out to be sensitive to the modeling assumptions concerning both the effects of the local chemical composition and the external elastic strains.

Kinetic Monte Carlo modeling demonstrates an abundance of relaxation patterns, arising from variations of the metal interaction energies within reasonable limits, compatible with the uncertainties of the approaches tested by *ab initio*. Depending on the In content in the matrix and the particular parameter sets used, linear or wall ordering of In and Ga atoms along the *c* axis, various planar ordering patterns parallel to basal plane, and spinodal decomposition have been observed.

This high sensitivity of the GaInN decomposition to relatively small variations of the interaction between Ga and In atoms seems to be the main reason for the experimentally observed versatility of the alloy decomposition patterns and their sensitivity to the particular experimental conditions.

ACKNOWLEDGMENTS

This research has been supported by the Academy of Finland through the Centers of Excellence program (2006-2011) and by Grants No. 06-08-81030 and No. 06-08-81031 from the Russian Foundation for Basic Research. We also wish to thank the Center for Scientific Computing (Helsinki, Finland) for the use of their computational facilities.

[1] S. J. Pearton, J. C. Zolper, R. J. Shul, and F. Ren, J. Appl. Phys. **86**, 1 (1999).
[2] K. Osamura, S. Naka, and Y. Murakami, J. Appl. Phys. **46**, 3432 (1975).
[3] R. Singh and T. D. Moustakas, Mater. Res. Soc. Symp. Proc. **395**, 163 (1996).
[4] R. Singh, D. Doppalapudi, T. D. Moustakas, and L. T. Romano, Appl. Phys. Lett. **70**, 1089 (1997).
[5] T. Matsuoka, Proceedings of the Second International Conference on Nitride Semiconductors (Elsevier, Amsterdam, 1997), p. 19.
[6] N. A. El-Masry, E. L. Piner, S. X. Liu, and S. M. Bedair, Appl. Phys. Lett. **72**, 40 (1998).
[7] M. D. McCluskey, L. T. Romano, B. S. Krusor, D. P. Bour, N. M. Johnson, and S. Brennan, Appl. Phys. Lett. **72**, 1730 (1998).
[8] P. Ruterana, G. Nouet, W. Van Der Stricht, I. Moerman, and L. Considine, Appl. Phys. Lett. **72**, 1742 (1998).
[9] D. Doppalapudi, S. N. Basu, K. F. Ludwig, and T. D. Moustakas, J. Appl. Phys. **84**, 1389 (1998).
[10] D. Doppalapudi, S. N. Basu, and T. D. Moustakas, J. Appl. Phys. **85**, 883 (1999).
[11] M. K. Behbehani, E. L. Piner, S. X. Liu, N. A. El-Masry, and S. M. Bedair, Appl. Phys. Lett. **75**, 2202 (1999).
[12] Z. Liliental-Weber, D. N. Zakharov, K. M. Yu, J. W. Ager III, W. Walukiewicz, E. E. Haller, H. Lu, and W. J. Schaff, Physica B **376-377**, 468 (2006).
[13] N. Weiser, O. Ambacher, H.-P. Felsl, L. Görgens, and M. Stutzmann, Appl. Phys. Lett. **74**, 3981 (1999).
[14] A. Zunger and S. Mahajan, in *Handbook on Semiconductors*, edited by S. Mahajan (North-Holland, Amsterdam, 1994), Vol. 3B p. 1399.
[15] J. E. Northrup, L. T. Romano, and J. Neugebauer, Appl. Phys. Lett. **74**, 2319 (1999).
[16] E. Zielinska-Rohozinska, J. Gronkowski, M. Regulska, M. Majer, and K. Pakula, Cryst. Res. Technol. **36**, 903 (2001).
[17] G. B. Stringfellow, J. Cryst. Growth **58**, 194 (1982).
[18] J. L. Martins and A. Zunger, Phys. Rev. B **30**, 6217 (1984).
[19] I. H. Ho and G. B. Stringfellow, Appl. Phys. Lett. **69**, 2701 (1996).
[20] T. Matsuoka, Appl. Phys. Lett. **71**, 105 (1997).
[21] A. Wakahara, T. Tokuda, X.-Z. Dang, S. Noda, and A. Sasaki, Appl. Phys. Lett. **71**, 906 (1997).
[22] L. K. Teles, J. Furthmüller, L. M. R. Scolfaro, J. R. Leite, and F. Bechstedt, Phys. Rev. B **62**, 2475 (2000).
[23] F. Grosse and J. Neugebauer, Phys. Rev. B **63**, 085207 (2001).
[24] A. K. Singh, V. Singh, and S. Lele, Acta Metall. Mater. **39**, 2847 (1991).
[25] M. Shimotomai and A. Yoshikawa, Appl. Phys. Lett. **73**, 3256 (1998).
[26] A. Cottrell, *An Introduction to Metallurgy*, 2nd ed. (Arnold, London, 1976).
[27] *Gallium Nitride and Related Semiconductors*, edited by J. H. Edgar, S. Strite, I. Akasaki, H. Amano, and C. Wetzel, EMIS Data Reviews, Vol. 23 (INSPEC, London, 1999).
[28] A. Tabata, L. K. Teles, L. M. R. Scolfaro, J. R. Leite, A. Kharchenko, T. Frey, D. J. As, D. Schikora, K. Lischka, J. Furthmüller, and F. Bechstedt, Appl. Phys. Lett. **80**, 769 (2002).

[29] L. K. Teles, L. G. Ferreira, L. M. R. Scolfaro, and J. R. Leite, Phys. Rev. B **69**, 245317 (2004).
[30] K. Laaksonen, M. G. Ganchenkova, and R. M. Nieminen, Physica B **376-377**, 502 (2006).
[31] M. E. J. Newman and G. T. Barkema, *Monte Carlo Methods in Statistical Physics* (Clarendon, Oxford, 1999).
[32] G. Kresse and J. Furthmüller, Comput. Mater. Sci. **6**, 15 (1996).
[33] J. P. Perdew and A. Zunger, Phys. Rev. B **23**, 5048 (1981).
[34] G. Kresse and D. Joubert, Phys. Rev. B **59**, 1758 (1999).
[35] H. J. Monkhorst and J. D. Pack, Phys. Rev. B **13**, 5188 (1976).
[36] E. J. Miller and E. T. Yu, Appl. Phys. Lett. **78**, 2303 (2001).
[37] M. G. Ganchenkova and R. M. Nieminen, Phys. Rev. Lett. **96**, 196402 (2006).
[38] M. G. Ganchenkova, S. Nicolaysen, V. A. Borodin, E. Halvorsen, and R. M. Nieminen, Mater. Sci. Eng., B **134**, 245 (2006).
[39] M. G. Ganchenkova and V. A. Borodin, Mater. Sci. Semicond. Process. **9**, 507 (2006).